Materials Characterization 120 (2016) 257–262

Contents lists available at ScienceDirect

Materials Characterization

journal homepage: www.elsevier.com/locate/matchar

RETRACTED

# A study approach on ferroelectric domains in $BaTiO_3$

L.S.R. Rocha [a], C.S. Cavalcanti [a], R.A.C. Amoresi [b,*], B.D. Stojanovic [c], E. Borsari [a], M.A. Za[illegible]ete [b], [illegible] Simões [a]

[a] Faculty of Engineering of Guaratinguetá, São Paulo State University - UNESP, Guaratinguetá, SP, Brazil
[b] Interdisciplinary Laboratory of Electrochemistry and Ceramics, LIEC – Department of Chemistry Techonology, Chemistry Institute, São Paulo State University - UNESP, Araraquara, SP, Brazil
[c] Institute for Multidisciplinary Research, University of Belgrade, Kneza Viselava 1, 11000 Belgrade, Serbia

ARTICLE INFO

*Article history:*
Received 6 April 2016
Received in revised form 5 September 2016
Accepted 10 September 2016
Available online 12 September 2016

*Keywords:*
Ceramics
Crystal growth
Piezoelectricity

ABSTRACT

Atomic Force Acoustic Microscopy (AFAM) and Piezo Response Force Microscopy (PFM) were used to study local elastic and electromechanical response in $BaTiO_3$ ceramics. A commercial multi-mode Scanning Probe Microscopy (SPM) and AFAM mode to image contact stiffness were employed to accomplish the aforementioned purposes. Stiffness parameters along with Young's moduli and piezo coefficients were quantitatively determined. PFM studies were based on electrostatic electromechanical response from localized tip-surface contact. Comparison was made regarding the Young's moduli obtained by AFAM and PFM. In addition, phase and amplitude images were analyzed based on [illegible]ng behavior, obtained via the application of −10 V to +10 V local voltage.



## 1. Introduction

Barium titanate ($BaTiO_3$) has been extensively employed in several industrial applications, including dynamic random access memory (DRAM) capacitor, microwave filters, infrared detectors, and dielectric phase shifters, owing largely to their excellent ferroelectric, piezoelectric and pyroelectric properties [1–8]. For $ABO_3$ perovskite, different A-site and B-site dopants (where A = Ca, Sr, B = Nb, Ta, Zr) are used aiming at modifying the [illegible] properties of $BaTiO_3$ based compositions [1–9].

As widely acknowledged, oxides and nitride-based piezo materials are used in electronic device applications including MEMS, FeRAMs and other ferroelectric heterostructures [10–11]. An understanding of local ferroelectric properties such as strong coupling between electrical and mechanical response at the nanometer level will undoubtedly enhance the functionality of these materials. Scanning probe techniques are, by and large, employed [illegible] at gaining understanding of the local ferroelectric behavior on such length scales. Atomic Force Acoustic Microscopy (AFAM) and Piezoresponse Force Microscopy (PFM) are among the [illegible] relevant Scanning Probe Microscope (SPM)-based techniques which are capable of evaluating ferroelectric properties on nanoscale [12–18]. These techniques allow the imaging of ferroelectric domains architecture at ~10 nm level while providing direct information on localized electromechanical activity. Chen et al. have studied the research progress on ferroelectric domains of lead-free films with relatively good ferroelectric and piezoelectric response which have been attributed to the films well-defined domain structure [19]. In a [illegible] work, the authors were able to improve the magnetic coupling of $BiFeO_3/Bi_4Ti_3O_{12}$ composite obtained by a chemical solution deposition with desirable ferroelectric, piezoelectric and dielectric responses as well as low leakage current, paving the way towards its future application in sensors and spin devices. These results are essentially associated with a strong coupling between ferroelectric and ferromagnetic orders as a result of the coexistence of different domain structures of this composite [20].

Based on these facts, we will conduct a systematic study approach of a lead-free bulk system composed of $BaTiO_3$ (*BT*), which is a ferroelectric material found to exhibit excellent piezoelectric behavior, resulting in wide applications in electronic control systems. *BT* possesses high dielectric constant and, generally, good ferroelectric properties. The study of ferroelectric domain behavior is seen to be of vital significance in view of the current upsurge of interest in multiferroic materials [3–8]. To achieve the desired properties, *BT* primarily needs to be free of intermediate crystalline phases, with a defined stoichiometry and a homogeneous microstructure. It is noteworthy that a wide range of preparation methods for *BT* have been investigated. The solid state reaction, starting from $BaCO_3$ or BaO, and $TiO_2$, has been shown to be suitable for the preparation of *BT* ceramics with high performance application as the resulting material exhibits large particle size and grain growth [21]. The main constraint of the solid state reaction lies in the fact that it requires repeated heat treatments besides grinding and contamination often becomes a problem [22]. This paper presents the results of the studies conducted using Atomic Force Acoustic Microscopy (AFAM) and Piezo Force Microscopy (PFM) to monitor the organization of local ferroelectric domains in $BaTiO_3$ ceramic pellets prepared by solid state reaction with careful control of impurities. In addition, electromechanical coupling related to elastic and piezo properties of the material were also thoroughly assessed. Elastic constant and piezo coefficient were

* Corresponding author.
*E-mail address:* rafaelciola@yahoo.com.br (R.A.C. Amoresi).

http://dx.doi.org/10.1016/j.matchar.2016.09.015
1044-5803/

RETRACTED

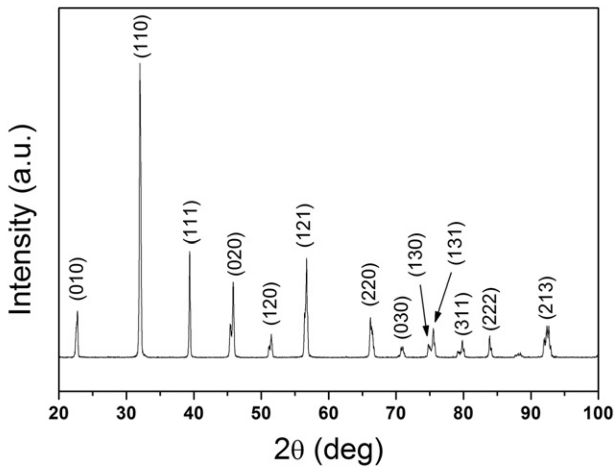


**Fig. 1.** XRD pattern of the $BaTiO_3$ pellet prepared via solid state reaction.

calculated. AFAM and PFM responses were investigated at various zones of the barium titanate pellets. Furthermore, a point-by-point mapping of piezospectroscopic behavior was carried out [23,24].

## 2. Experimental Procedure

$BaTiO_3$ (BTO) samples were synthesized by solid state reaction. The barium titanate was prepared starting from barium oxide (BaO) and titanium oxide ($TiO_2$), in a rutile crystal form (Fluka, 99.8% purity). BaO was obtained from $BaCO_3$ (E. Merck, 99.0% purity) according to the following reaction: $BaCO_3 \rightarrow BaO + CO_2$ in air at 900 °C/4 h. After polishing, AFM studies using different modes were carried out through SPM with Nanoscope IV controller equipped with standard silicon nitride tips coated with gold-cadmium. The typical force constant of these tips was 0.09 N/m and the apex radius was 20–40 nm. The AFM methodology, which is useful for obtaining local elasticity images, has been previously discussed in the literature [9,25,26]. This principle was optimized so as to evaluate local mechanical properties of the $BaTiO_3$ pellet. AFM measurements were carried out in contact mode. A conducting AFM tip was used to apply an AC voltage superimposed with a DC bias for computing piezo activit[illegible] variation in the direction of domain orientation is achieved by controlling the magnitude of impressed voltage [9–11,27,28]. PFM spectroscopy was carried out for the bias voltage within the range of [illegible] V to +[illegible] V aiming at studying piezoresponse and polarization exhibited in different regions. The piezoresponse from ferroelectric materials was investigated by PFM with a resolution of 10 nm. The applied voltage was a combination of a DC bias and an alternating voltage that resulted in cantilever deflection. The PFM image was obtained at a frequency of ~790 kHz.

The acoustic vibration of the specimen was maintained at 2.25 MHz. In order to cover the complete range of the flexural vibrations of the cantilever, the employed frequency was changed from 10 kHz to 2 MHz. Amplitude and frequency shifts resulting from coupled oscillations were recorded following mapping. Similarly, stiffness constants were derived from force-distance curves. Contact resonance frequency curves in AFAM studies on $BaTiO_3$ pellet were recorded. This method

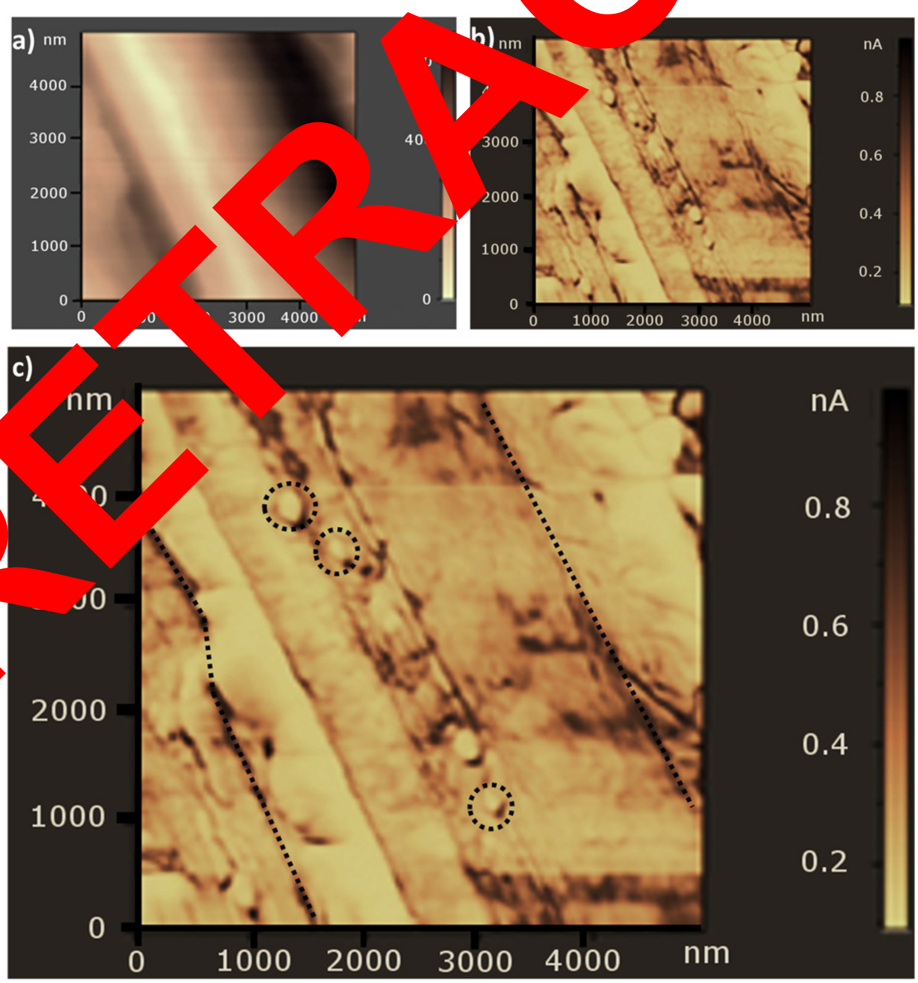


**Fig. 2.** Comparison between topography (a) and resonance frequency image (b) of the $BaTiO_3$ pellet surface.

has been described earlier [3–9]. For the sake of clarity, the following mathematical expression was used:

$$k^*_{BaTiO_3} = k^*_{Si}\frac{\left[f^2_{BaTiO_3} - f^2_{Si}\right]}{\left[f^2_{Si} - f^2_0\right]} \quad (1)$$

where

$k^*_{BaTiO3}$: contact stiffness of the sample pellet,
$k^*_{si}$: contact stiffness of the Silicon wafer (used as reference),
$f^*_{BaTiO3}$: contact resonance frequency of the sample pellet,
$f^*_{Si}$: contact resonance frequency of the Si wafer and,
$f_0$: free resonance frequency of the cantilever.

These calculations were made after recording resonance spectra.

## 3. Results and Discussion

Fig. 1 shows the XRD patterns for the $BaTiO_3$ pellet prepared via solid state reaction. The Bragg peaks indicate the crystallization of BT perovskite phase with *P4mm* space in the crystalline tetragonal structure (JCPDS card no. 05-0626). It is worth noting that no secondary or intermediate carbonate phases were observed. The absence of $BaCO_3$ can be attributed to complete reaction. Perovskite $BaTiO_3$ phase was seen to be well-crystallized implying the occurrence of the solid state reaction while the nucleation and subsequent growth of perovskite crystallites were found to be favored at 900 °C/4 h.

Fig. 2a–b illustrates the topography and acoustic mode in resonance frequency acquired simultaneously. Topography image (Fig. 2a) was mapped in *AFM* contact mode, where large grains in the forn[illegible] umns are observed devoid of pores. In Fig. 2b, the acoustic ima[illegible] enables the visualization of the grains substructures. The selected [illegible]ue of the excitation frequency was 2.25 MHz which is a[illegible] the co[illegible] resonance (10 kHz–2 MHz). Thus, stiffer regions [illegible] brigh[illegible] The acoustic images are formed by a columns pa[illegible] with [illegible]ite strip[illegible] parallel along the dark stripes, typical of polari[illegible]n 180° [illegible] axis of the crystal [29,30]. Fig. 2c is an enlarged a[illegible] of [illegible] the grain boundaries and white stripes for[illegible] by smal[illegible]s characteristic of substructures marked in dashed [illegible] These substru[illegible]es are stiffer structures formed by nanograins [illegible] th[illegible]ntours comp[illegible]sed of ferroelectric domains along them. Quantitativ[illegible]lysis of the stiffness in those zones was carried [illegible]using referenc[illegible]ples such as Si and PZT. Furthermore, the A[illegible]M image depicts regu[illegible]r and irregular "fingerprint-like" domai[illegible]ttern [illegible]arious zones on the pellet surface. The large zones with st[illegible]ain in th[illegible] image are actually consisted of smaller doma[illegible]tructu[illegible]elow 50[illegible]. Guided by the aim of studying the beha[illegible]se dom[illegible]r electric field, PFM studies were performe[illegible]bservi[illegible] the doma[illegible]witching and are described in the next su[illegible]ction.

Fig. 3a[illegible]ucture of the pellet in different regions showing the [illegible]ndence of the deflection with distance. The obtained curves clearly s[illegible] distinct inclinations, as the pink curve deflection decreases continu[illegible]sly even after the detachment from the center (zero), while the green curve remains constant during extension and retraction of the tip. Such behavior is a reflection of heterogeneity in several regions caused by different surface rigidity. Using reference samples, stiffness constants for several coupled systems were quantitatively determined, and are given in Table 1. Contact resonance spectra from few representative points on $BaTiO_3$ surface are shown in Fig. 3b. The mechanical spectrum is influenced by the elastic and viscous behavior of the sample once the tip stiffness is constant. Significant changes in frequency and magnitude of the contact resonance ranging from 1290 kHz to 1337 kHz between the various locations can be clearly noted. The larger vibrational frequency of the spectra implies a decrease in its vibrational wavelength of interaction caused by stiffer region of

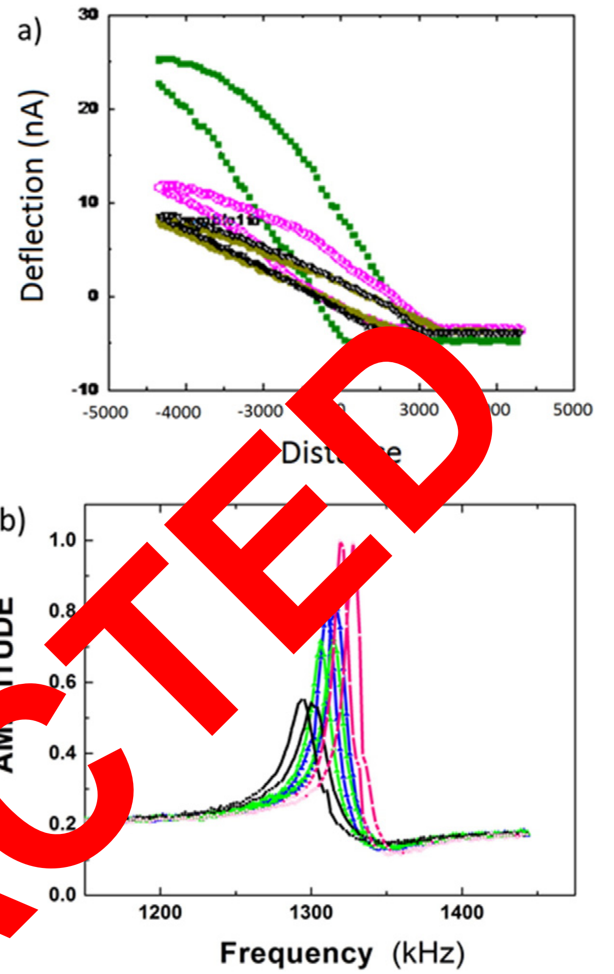


**Fig. 3.** a) Force curves and b) contact resonance frequencies for various points on the surface of $BaTiO_3$ pellet.

the sample. The amplitude, which is related to the energy dissipation of the interaction, must be evaluated by the full width at half maximum (FWHM) of the peaks, where softer regions exhibit broader peaks followed by a reduction in amplitude. The shape of the peak in doublet can be represented by two springs in series representing elastic behavior among the cantilever-sample interactions [31]. Stiffness constants as well as resonance peak shifts are used in the evaluation of Young's modulus (E) [6–9] according to Eqs. (2) and (3):

$$E^*_{BaTiO_3} = E^*_{Si}\left(\frac{k^*_{BaTiO_3}}{k^*_{Si}}\right)^{3/2} \quad (2)$$

$$\frac{1}{E^*} = \frac{1-\nu^2_{tip}}{E_{tip}} + \frac{1-\nu^2_{BaTiO_3}}{E_{BaTiO_3}} \quad (3)$$

Estimated moduli evaluated using these formulations, are given in Table 2.

**Table 1**
Values of effective stiffness and elastic constants for sample and reference materials.

| Coupled system | F (nN) | K* (N/m) ± 10% | E* (×$10^{10}$ N/$m^2$) ± 10% |
|---|---|---|---|
| Si-$W_2C$ | 250 | 11.3 | 5.6 |
| PZT-$W_2C$ | 300 | 10.5 | 4.2 |
| BTO-$W_2C$ | 300 | 22.3 | 14.4 |

**Table 2**
Elastic modulus and Poisson's coefficients for various materials.

| Materials | E ($\times 10^{10}$ N/m$^2$) reported | $\nu$ | E ($\times 10^{10}$ N/m$^2$) |
|---|---|---|---|
| Si | 11.8 | 0.28 | 10.3 |
| PZT | 10.2 | 0.29 | 6.2 |
| $BaTiO_3$ | 13.7 | 0.27 | 16.5 |

To improve contrast in the *AFAM* image, and to enable investigation of finer features, the image was mapped at two different frequencies, below (Fig. 4a) and above (Fig. 4b) the resonance frequency. In Fig. 4a, the mapping below resonance frequency clearly shows bright and dark regions, where bright regions indicate soft zones while dark ones correspond to hard zones. Similarly, AFAM image was mapped at a frequency above resonance value, which is shown in Fig. 4b, where the hard and soft zones found here point to contrast inversion, through which the axis of orientation measured in the unit cell is dependent on the tip probe. Through the dotted arrows, in Fig. 4a and Fig. 4b, one can clearly observe the presence of substructures, having different contrasts according to the applied resonance contrast indicating variation in contact stiffness [7–9]. Domains with average size of ~50 nm bearing different values of stiffness are clearly visible. Fig. 4c shows topography while poling. The corresponding piezoresponse image (using magnitude signal mapping, in the PFM mode), obtained by adjusting various DC bias voltages, ranging from −10 V to +10 V for different times, is given in Fig. 4d. The image indicates that the perpendicular component of polarization can be switched between two stable states: bright and dark. The piezoelectric response component in the out of plane direction is represented by a line profile during poling, as shown in Fig. 4e, which is a reference of the lines depicted in Fig. 4c–d. Such behavior, in effect, corresponds to the different orientations of polarized domains. Dark regions with higher current correspond to domains oriented in the same direction of the polarization axis (soft domains), while bright regions are related to domains perpendicular to the polarization axis, which explains their reason of having lower current (hard domains).

For a much thorough comprehension of the system, the piezoelectric vibrations were monitored through of the observation of the amplitude, which is connected to the piezoelectric coefficient of the material. Similarly, the phase of the signal is capable of revealing the polarization direction. Fig. 5a shows PFM images along with topography, with area ~ 10 × 10 μm$^2$, for different regimes present in the area. The amplitude of the piezoelectric vibration is shown in Fig. 5b, the bright area illustrates the piezoelectrically active region parallel to the applied electric field while dark regions are associated with piezoelectrical activities oriented in the opposite direction of the applied field on the pellet surface. Phase image (Fig. 5c) clearly shows the polarization direction in different zones at various voltages and the topmost and bottommost areas in the image have the same value. The observed piezo domains are attributed to the inverse piezoelectric effect on the material surface. Applied voltage is shown to cause the electromechanical realignment of the domains. This switching behavior was monitored by locally applying voltages between −10 V and +10 V [13–14]. Corresponding to these voltages, changes in tune of approximately 40% were observed in the phase- and amplitude-contrast images. In these images at various points, piezospectroscopy was carried out.

In order to achieve quantitative analysis of the PFM data, the electroelastic field distribution was obtained. By meticulous observation, it was found that a hysteresis loop could be obtained using a stiff tip at several points on the surface. Fig. 6 shows the piezo response using amplitude and phase signals as a function of bias voltage at a typical point. Fig. 6a shows the typical piezoresponse amplitude of the pellet immediately while applying −10 V to +10 V DC biases over the scanned region by the AFM tip, along the direction perpendicular to the in-plane. The maximum piezoresponse signal seen in the butterfly loop is shifted left by 0.3 V. This may be associated with different work functions existing between the two electrodes, i.e. the tip and the bottom plate. Above 6 V, the value of piezoresponse is found to be almost flat. Apart from the magnitude, the sign of the piezo response, which is related to the polarization direction of a zone point on the surface, is seen to undergo a change. Fig. 6b shows the piezoresponse phase

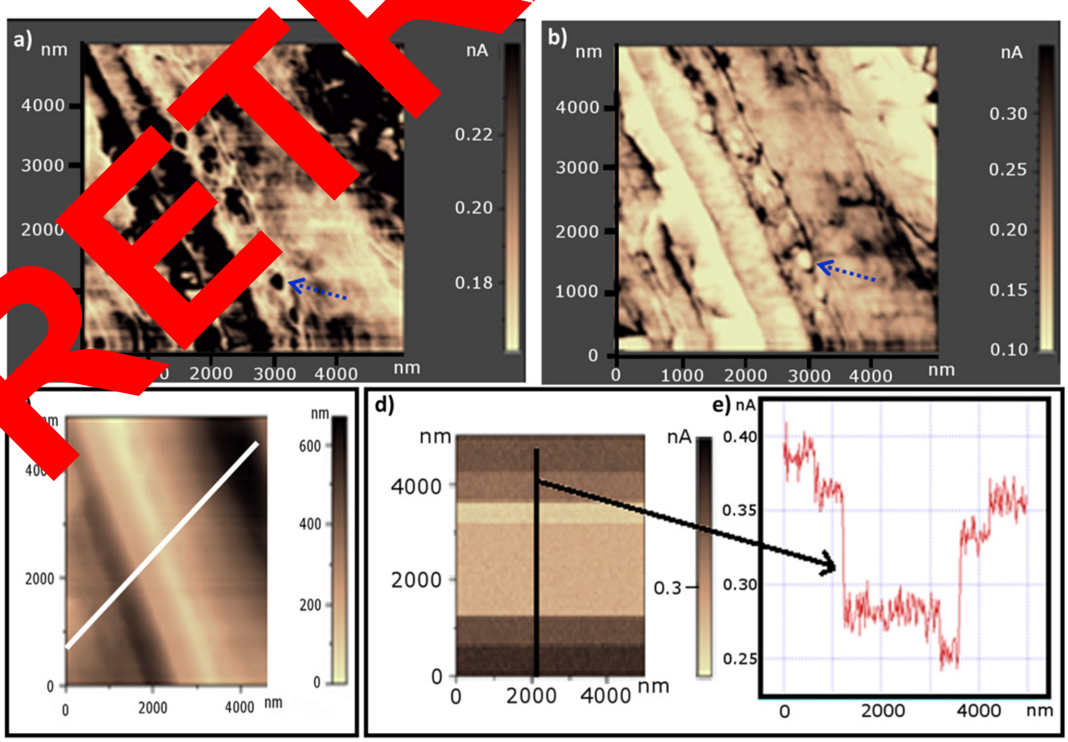


**Fig. 4.** AFAM images below (a) and above (b) the resonance frequency. AFAM image while/during poling (c). Piezoresponse (magnitude signal mapping) image (d) while poling using various DC bias voltages ranging from −10 V to +10 V at different durations and line profile during poling (e).

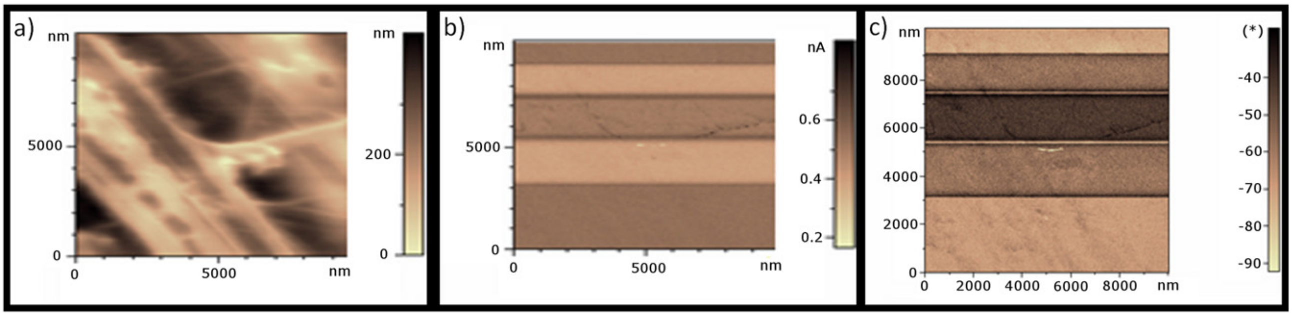

**Fig. 5.** Topography during poling (a), PFM amplitude (b) and PFM phase (c) images during poling while applying different DC bias, with voltage ranging from −10 V to +10 V.

RETRACTED

as a function of the applied DC voltage. It reveals the phase difference of the detected signal existing between positive and negative voltages. By combining the amplitude loop (i.e. butterfly loop and phase loop), one can obtain the hysteresis loop. Fig. 6c illustrates the piezoelectric hysteresis loop response of the $BaTiO_3$. Characteristic loop is known to be dependent mainly on the properties of the pellet. The comparative inferences and observations of AFAM and PFM are discussed below.

Based on the AFAM studies at various resonance frequencies, the images are clearly noted to be very informative regarding the grains, grain boundaries and domain architecture. A wide range of domains shapes and sizes are clearly seen. Stiffness variation over the surface is about <12%, which may be attributed to the grain, grain boundaries and domains. In addition, microscopically, this variation of stiffness can arise from pellet parameters such as surface roughness. A further observation worth mentioning is that the BTO pellet surface is found to be harder compared to those of Si and PZT (Table 2). Variation in E may stem from different zones having varying elasticities. Distribution of E (between 14 and 18 × $10^{10}$ N/$m^2$) in the polished pellet is seen to be influenced by their morphology. In PFM, the total force acting on the AFM tip is a combination of two forces. One of these forces is the elastic force exerted by the cantilever with a constant spring k at deflection position $d_0$. The other force denoted as $F_{el}$ is the electrostatic force; the latter force is modulated by a sinusoidal voltage superimposed with a DC component, cantilever response varies according to variation related to electrical and mechanical-(elastic) properties of the surface. Hence, cantilever response, based on surface electromechanical interaction, changes with bias voltages. As reported in the literature [3–7], an approximate value of piezocoefficient is calculated to be about ~9 × $10^{-11}$ m/V, which is almost 50% of that of the PZT pellet. Elastic constant (E ~ 14.3 × $10^{10}$ N/$m^2$) was estimated through a relation derived by Kalinin [illegible] and Harapetian [32] which employed piezocoefficient and Young's moduli for polycrystalline materials within the electromechanical regime, bringing the tip into contact with the surface, generating a first-harmonic component of bias-induced tip deflection $d = d_0 + A\cos(\omega t + \varphi)$ with the phase yielding information on the polarization direction below the tip. For $c^-$ domains with polarization vector pointing downwards, the application of a positive bias tip causes surface oscillations expansion of the sample, as such the phase with the [illegible] voltage thus $\varphi = 0$. And for $c^+$ domains with polarization vector pointing upward, $\varphi = 180°$ [22]. The amplitude A defines the local electromechanical response and depends on the geometry of the tip-surface junction and materials properties, whose mathematical descriptions are deemed extremely complex to ascertain. Comparison was made between E values obtained by AFM and PFM. Further improvements in these studies ought to be done through the enhancement of pellet density, morphology and electrical contacts. In further studies, our intention is to have a metallic electrode film on both sides of the pellet and/or a film to reduce the working function as well as contact problems.

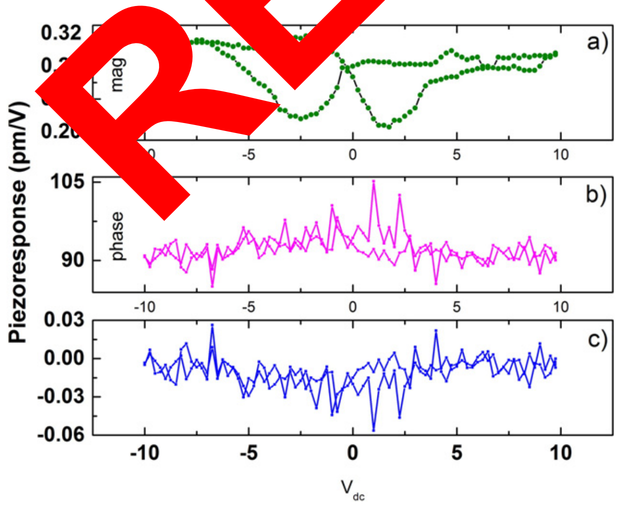


**Fig. 6.** Piezoresponse at a typical point on the pellet surface.

## 4. Conclusions

To aid our understanding of the nanoscale behavior of piezo domains in $BaTiO_3$ ferroelectric materials, AFAM and PFM studies were successfully executed. In AFM, height images give us a hint regarding the roughness variation along with topography for the test and reference samples. Topography and AFAM images clearly indicate the stiffness variation on nanoscale in substructures within the grains. Below 50 nm, ferroelectric domains with different values of stiffness were clearly observed in the AFAM image of the pellet. Quantifications of stiffness and elastic constants were carried out using standard reference samples such as Silicon and PZT. The spatial inhomogeneity of ferroelectric domain structure reveals that the random internal field observed is attributed to the nanoscale structural irregularities on the material. Under PFM mode, piezoresponse of domains with respect to the applied electric field was investigated. Electromechanical realignment of the domains was observed during poling.

## Acknowledgements

The authors would like to express their warm gratitude to Dr. Ramesh for his useful discussions on AFAM and PFM at various stages of the research. The authors do acknowledge the sustained encouragement and financial support provided by CNPq (573636/2008-7), INCTMN (2008/57872-1) and FAPESP (2013/07296-2) research funding agencies. Our thanks also go to Brian Newmann – the English language content editor for his painstaking editing and proofreading of the manuscript.

## References

[1] H.Y. Tian, Y. Wang, J. Miao, H.L.W. Chan, C.L. Choy, Preparation and characterization of hafnium doped barium titanate ceramics, J. Alloys Compd. 431 (2007) 197–202.

[2] J.Y. Chen, Y.W. Tseng, C.L. Huang, Improved high Q value of (1 − x)Ca(Mg1/3Ta2/3)O3–xCa0·8Sm0.4/3TiO3 solid solution with zero temperature coefficient of resonant frequency, J. Alloys Compd. 494 (2010) 205–209.

[3] F. Boujelben, F. Bahri, C. Boudaya, A. Maalej, H. Khemakhem, A. Simon, M. Maglione, Effect of Ni doped BaTiO3 on the dielectric properties in the Ba(Ni1/3Nb2/3)xTi1 − xO3 solid solution, J. Alloys Compd. 481 (2009) 559–562.

[4] Q. Xu, X.F. Zhang, Y.H. Huang, W. Chen, H.X. Liu, M. Chen, B.H. Kim, Effect of MgO on structure and nonlinear dielectric properties of Ba0·6Sr0.4TiO3/MgO composite ceramics prepared from superfine powders, J. Alloys Compd. 488 (2009) 448–453.

[5] O.P. Thakur, P. Chandra, A.R. James, Enhanced dielectric properties in modified barium titanate ceramics through improved processing, J. Alloys Compd. 470 (2009) 548–551.

[6] H.I. Hsiang, C.S. Hsi, C.C. Huang, S.L. Fu, Sintering behavior and dielectric properties of BaTiO3 ceramics with glass addition for internal capacitor of LTCC, J. Alloys Compd. 459 (2008) 307–310.

[7] Z.G. Hu, Y.W. Li, M. Zhu, Z.Q. Zhu, J.H. Chu, Microstructural and optical investigations of sol–gel derived ferroelectric BaTiO3 nanocrystalline films determined by spectroscopic ellipsometry, Phys. Lett. A 372 (2008) 4521–4526.

[8] S.F. Wang, Y.R. Wang, Y.C. Wu, Y.J. Liu, Densification, microstructural evolution, and dielectric properties of hexagonal Ba(Ti1 − xMnx)O3 ceramics sintered with fluxes, J. Alloys Compd. 480 (2009) 449–504.

[9] M. Cernea, E. Andronescu, R. Radu, F. Fochi, C. Galassi, Sol–gel synthesis and characterization of BaTiO3-doped (Bi0·5Na0.5)TiO3 piezoelectric ceramics, J. Alloys Compd. 490 (2010) 690–694.

[10] A. Gruverman, O. Auciello, H. Tokumoto, Imaging and control of domain structures in ferroelectric thin films via scanning force microscopy, Annu. Rev. Mater. Sci. 28 (1998) 101–123.

[11] A. Moulson, H. JM, Electroceramics: Materials, Properties, Applications, Chapman and Hall, London, 1990.

[12] E. Kester, U. Rabe, L. Presmanes, P. Tailhades, W. Arnold, Measurement of Young's modulus of nanocrystalline ferrites with spinel structures by atomic force acoustic microscopy, J. Phys. Chem. Solids 61 (2000) 1275–1284.

[13] S.V. Kalinin, D.A. Bonnel, Imaging mechanism of piezoresponse force microscopy of ferroelectric surfaces, Phys. Rev. B 65 (2002) (125408-1-11).

[14] T. Stoica, R. Calacro, R. Meijers, H. Lüth, Nanoscale imaging of surface piezoresponse of GaN epitaxial layers, Appl. Surf. Sci. 253 (2007) 4300–4306.

[15] S.V. Kalinin, D.A. Bonnell, Atomic polarization and local reactivity on ferroelectric surfaces: a new route toward complex nanostructures, Nano Lett. 2 (2002) 589–593.

[16] U. Rabe, V. Scherer, S. Hirsekorn, W. Arnold, Nanomechanical surface charact[illegible]tion by atomic force acoustic microscopy, J. Vac. Sci. Technol. B 15 [illegible] 1506–1511.

[17] U. Rabe, S. Amelio, E. Kester, V. Scherer, S. Hirsekorn, W. Arnold, Quantitative determination of contact stiffness using atomic force acoustic microscopy, Ultrasonics 38 (2000) 430–437.

[18] M. Prasad, M. Kopycinska, U. Rabe, W. Arnold, Measurement of Young's modulus of clay minerals using atomic force acoustic microscopy, Geophys. Res. Lett. 29 (2002) 13-1–13-4.

[19] J. Chen, Z. Tang, R. Tian, Y. Bai, S. Zhao, H. Zhang, Domain switching contribution to the ferroelectric, fatigue and piezoelectric properties of lead-free Bi0.5(Na0.85 K0.15)0.5TiO3 films, RSC Adv. 6 (2016) 33834.

[20] J. Chen, Z. Tang, Y. Bai, S. Zhao, Multiferroic and magnetoelectric properties of BiFeO3/Bi4Ti3O12 bilayer composite films, J. Alloys Compd. 675 (2016) 257–265.

[21] P. Guthner, K. Dransfeld, Local poling of ferroelectric polymers by scanning force microscopy, Appl. Phys. Lett. 61 (1992) 1137–1139.

[22] S.V. Kalinin, E. Karapetian, M. Kachanov, Nanoelectromechanics of piezoresponse force microscopy, Phys. Rev. B 70 (2004) (184101-1-24).

[23] Q.X. Jia, H.H. Kung, X.D. Wu, Microstructure proper[illegible]0·5Sr0.5TiO3 thin films on Si with conductive SrRuO3 bottom electr[illegible] Films 299 (1997) 115–118.

[24] B.L. Newalkar, S. Komarneni, Microwave-[illegible]hermal synthe[illegible]d characterization of barium titanate powders, Mater. Res. [illegible]36 (2001) 23[illegible]355.

[25] G. Mangamma, B. Ramachandran, T.[illegible]airam, [illegible]amachand[illegible]o, S. Dash, A.K. Tyagi, Imaging of nanometric fe[illegible]ectric doma[illegible] BaTiO[illegible]ng atomic force acoustic microscopy and pie[illegible]ce microscopy, [illegible]osc. Res. 6 (2011) 29–34.

[26] T. Stoica, R. Calarco, R. Mei[illegible] Luth[illegible]oscale imaging of surface piezoresponse on GaN epitaxial laye[illegible] Appl[illegible]53 (2007) [illegible]0–4306.

[27] L.M. Eng, H.J. Günth[illegible], G.A. S[illegible]der, U. Kö[illegible]J.M. Saldaña, Nanoscale reconstruction of surf[illegible]rystallograph[illegible] th[illegible]mensional polarization distribution in ferroe[illegible]rium-titanate c[illegible]Appl. Phys. Lett. 74 (1999) 233–235.

[28] K. Yamana[illegible] Na[illegible] Quantitative ela[illegible]city evaluation by contact resonance in an atomic f[illegible]ce micro[illegible] Appl. Phys. A Mater. Sci. Process. 66 (1998) S313–S317.

[29] V. Grubsky, S. MacCorm[illegible] Feinberg, All-optical three-dimensional mapping of 1[illegible]ns hidden in a [illegible] crystal, Opt. Lett. 21 (1996) 6–8.

[30] [illegible]othis, N.T. Tsou, J.E. Hube[illegible] review of domain modelling and domain imaging [illegible]chniques in ferroelectric crystals, Materials 4 (2011) 417–447.

[31] [illegible] Collins, A. Tse[illegible] S. Jesse, M.B. Okatan, R. Proksch, J.P. Mathews, G.D. Mitchell, B.J. [illegible]driguez, S.V. K[illegible]n, I.N. Ivanov, Breaking the limits of structural and mechanical [illegible]ing of the h[illegible]ogeneous structure of coal macerals, Nanotechnology 25 (2014) [illegible]

[32] E. K[illegible] Kachanov, S.V. Kalinin, Nanoelectromechanics of piezoelectric indentation and applications to scanning probe microscopy of ferroelectric materials, [illegible]ilos. Mag. 85 (2005) 1017–1051.